MNRAS **000**, 1–?? (2015) Preprint 20 April 2016 Compiled using MNRAS LATEX style file v3.0

Turbulence and Particle Acceleration in Giant Radio Halos: the Origin of Seed Electrons

Anders Pinzke[1,2⋆], S. Peng Oh[3] and Christoph Pfrommer[4⋆]
[1] *The Oskar Klein Centre for Cosmoparticle Physics, Stockholm University, AlbaNova University Center, SE - 106 91 Stockholm, Sweden*
[2] *Dark Cosmology Center, University of Copenhagen, Juliane Maries Vej 30, DK-2100 Copenhagen, Denmark*
[3] *University of California - Santa Barbara, Department of Physics, CA 93106-9530, USA*
[4] *Heidelberg Institute for Theoretical Studies (HITS), Schloss-Wolfsbrunnenweg 35, 69118 Heidelberg, Germany*

20 April 2016

ABSTRACT
About one third of X-ray-luminous clusters show smooth, unpolarized radio emission on ~Mpc scales, known as giant radio halos. One promising model for radio halos is Fermi II acceleration of seed relativistic electrons by compressible turbulence in the intracluster medium (ICM); Coulomb losses prohibit acceleration from the thermal pool. However, the origin of seed electrons has never been fully explored. Here, we integrate the Fokker-Planck equation of the cosmic ray (CR) electron and proton distributions in cosmological simulations of cluster formation. For standard assumptions, structure formation shocks lead to a seed electron population which produces too centrally concentrated radio emission. Instead, we present three plausible scenarios for the seed CRs that each can reproduce the spatially flat radio emission observed in the Coma cluster. (1) The CR proton-to-electron acceleration efficiency $K_{\rm ep} \sim 0.1$ is assumed to be larger than in our Galaxy ($K_{\rm ep} \sim 10^{-2}$), due to the magnetic geometry at the shock. The resulting primary electrons dominate the radio emission, which is more extended in comparison to radio emission from secondary electrons that result from hadronic CR interactions in the ICM. (2) CR protons may stream at the Alfvén speed to the cluster outskirts when the ICM is relatively quiescent. A spatially flat CR proton distribution develops and produces the required population of secondary seed electrons. (3) The ratio of injected turbulent-to-thermal energy density increases significantly with radius, as seen in cosmological simulations. This generates a flat radio profile when CRs are reaccelerated even if the seed population of CRs is steep with radius. These competing non-trivial solutions provide incisive probes of non thermal processes in the high-β ICM.

1 INTRODUCTION

About one third of X-ray-luminous clusters show smooth, unpolarized radio emission on ~Mpc scales, known as giant radio halos (RHs) (Brunetti & Jones 2014). They appear only in disturbed, merging clusters and the RH luminosity correlates with the X-ray luminosity (Govoni et al. 2001; Feretti et al. 2012) and the Compton y-parameter (Basu 2012; Planck Collaboration et al. 2013). The RHs show that CR electrons and magnetic fields permeate a large volume fraction of the intra-cluster medium (ICM). The dominant CR source, given the smoothness and enormous extent of RHs, is thought to be structure formation shocks (Miniati et al. 2001a; Pfrommer 2008). At the same time, plasma processes, the origin of magnetic fields and particle acceleration in a turbulent, high-β plasma like the ICM are not well understood. Radio halos thus provide an incisive probe of non-thermal processes in the ICM.

There have been two competing models proposed to explain RHs. The radio emitting electrons in the "hadronic model" are produced in inelastic (hadronic) CR proton interactions with protons of the ambient thermal ICM, which generates pions that eventually decay into electrons and positrons, depending of the charge of the initial pion (Dennison 1980; Blasi & Colafrancesco 1999; Miniati et al. 2001b; Pfrommer & Enßlin 2004a; Pfrommer et al. 2008; Enßlin et al. 2011). CR protons and heavier nuclei may have been accelerated and injected into the ICM by structure formation shocks, active galactic nuclei and galactic winds. However, the strong bimodality that separates X-ray luminous clusters into radio-active and radio-quite clusters (and requires a fast switch on/off mechanism of the RH emission) and the very extended RH emission at low frequencies in Coma (352 MHz) represent a major challenge to this model class (Brunetti et al. 2012; Zandanel et al. 2014).

The alternative model for RHs is re-energization of seed suprathermal electrons by Fermi II acceleration when ICM turbulence becomes transonic during mergers (Schlickeiser et al. 1987; Giovannini et al. 1993; Brunetti et al. 2001, 2004; Brunetti & Lazarian 2007, 2011; Miniati 2015). Due to the short radiative cooling time of

high-energy relativistic electrons, the cluster synchrotron emission quickly fades away after a merger, which naturally explains the observed bimodality of RHs (see e.g. Donnert et al. 2013; Donnert & Brunetti 2014).

However, there is a salient piece missing in the turbulent reacceleration model. It relies heavily on the assumption of an abundant, volume-filling population of seed suprathermal electrons; direct Fermi II acceleration from the thermal pool is precluded by strong Coulomb losses (Petrosian & East 2008; Chernyshov et al. 2012). These seeds are presumed to be either fossil CR electrons (CRes) accelerated by diffusive shock acceleration (DSA) during structure formation (Sarazin 1999), or secondaries injected by hadronic interaction of CR protons (CRps) with thermal protons (Brunetti & Lazarian 2011). While analytic estimates have been made, there has been no ab initio demonstration that structure formation can lead to the required abundance of seed electrons with the correct spatial and spectral characteristics. This is a non-trivial requirement: Coulomb cooling in dense cluster cores is severe, and DSA fossil electrons may not survive. On the other hand, for secondaries to constitute the seed population, the CRp population required in the best-studied case of the Coma cluster must have a very broad and flat (or even slightly inverted) spatial profile (Brunetti et al. 2012), in contrast with the thermal plasma whose energy density declines steeply with radius. In Fig. 1 we show that such a distribution is not predicted by cosmological simulations (see also Pinzke & Pfrommer 2010; Vazza et al. 2014). If CRps are predominantly advected with the cluster plasma, their distribution will be peaked towards the cluster center and shows a similar characteristics as the thermal plasma. As a consequence, the distribution of secondary electrons and the resulting radio synchrotron emission is also peaked since the hadronic reaction is a two-body scattering process (see Fig. 1). Hence, the simulated emission falls short of the observed extended and flat radio profile of the Coma cluster.

Indeed, arriving at a seed population with the required characteristics is highly constraining, and has the potential to teach us much about the origin of CRps/CRes in clusters. In this work, we use our hydrodynamical zoom simulations of galaxy clusters in a cosmological setting to follow the distribution functions of seed CRp and CRe population and integrate the Fokker-Planck equation of CR transport along Lagrangian particle trajectories. We resolve injection at structure formation shocks, account for various loss processes of CRs, and – most importantly – model second-order Fermi acceleration by CR interactions with magnetised turbulence. However, we assume a simplified and stationary model for magnetic fields and turbulence. We do not account for the time-varying energy density in compressible waves, which are thought to be necessary for the acceleration process (Brunetti & Lazarian 2007, 2011), as the cluster merger proceeds. So our approach is orthogonal (and complementary) to e.g., Miniati 2015. This enables us to vary parameters associated with the unknown continuation of magneto-hydrodynamical turbulence below the MHD scale and the overall amplitude of compressible waves.

In this paper we consider three new scenarios that individually or combined can reproduce the observed radio profiles and spectrum in the Coma cluster without violating gamma-ray constraints:

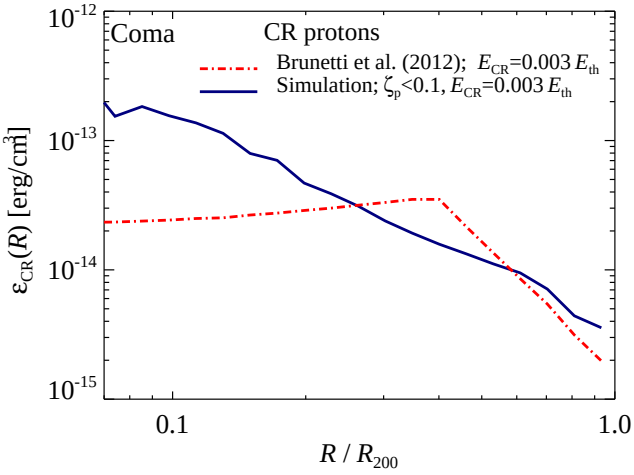

Figure 1. Spatial distribution of CRp energy density in the Coma cluster. The red dash-dotted line shows the required distribution of seed CRps that generate secondary electrons via p-p collisions required to reproduce Coma radio brightness observations after Fermi-II reacceleration (Brunetti et al. 2012). The blue solid line shows the distribution of fossil CRps found in cosmological simulations, which disagrees with the required profile. To better compare the two models in this figure, we normalize the required distribution of CRps by fixing the total CRp energy E_{CR} to 0.3 percent of the total thermal energy, consistent with observations (Ackermann et al. 2014; Arlen et al. 2012).

(i) **Model *M-primaries*.** If the acceleration efficiency of CRps is below about 0.1 % in weak (perpendicular) shocks and the ratio of injected electrons-to-protons $K_{ep} \sim 0.1$, this yields a dominant primary population with a flat spatial distribution, since primaries have a weaker density dependence than secondaries.

(ii) **Model *M-streaming*.** Here, we account for streaming CRps that produce flat distributions of CRps in the ICM (Enßlin et al. 2011; Wiener et al. 2013; Zandanel et al. 2014), which also flattens the secondary electron distribution.

(iii) **Model *M-turbulence*.** Here, we adopt a spatially flatter turbulent profile than what was adopted in Brunetti et al. (2012), but where seed CRps follow the steep profile that is suggested by structure formation simulations.

To pursue these three possibilities further, we employ cosmological simulations of CRs in clusters. In tandem with new insights from our recent work on DSA generated fossil electrons (Pinzke et al. 2013), we generate the first quantitative calculation of primary and secondary seed electrons and compare to observations in the Coma cluster. For the most part, we adopt parameters that are used in previous work: for details, see (Brunetti & Lazarian 2007, 2011, turbulent spectrum), (Miniati 2015, injection scale of turbulens), (Lau et al. 2009; Shaw et al. 2010; Vazza et al. 2011, energy density of turbulence), for CR acceleration in shocks, (Pinzke et al. 2013, in particular K_{ep}, acceleration efficiency), and for cosmological simulations, (Pinzke & Pfrommer 2010, i.e., shock history, temperature profile, density profile, magnetic field profile). All these parameters are uncertain, and could potentially change our predictions. We refere the reader to section 3 for a small

exploration of parameter space, however we leave the full exploration of parameter space and the interaction between free parameters to future work.

2 METHOD

The transport of relativistic electrons and protons in the ICM is a complex process that depends both on the details of the thermal component (gas density, temperature, and pressure) as well as non-thermal component (turbulence, magnetic fields, fossil CRs). We use high resolution galaxy cluster simulations to derive the thermal and fossil CR properties (shock accelerated primary CRes and CRps, as well as secondary CRes produced in p-p collisions) (Pfrommer et al. 2007; Pfrommer 2008; Pinzke & Pfrommer 2010; Pinzke et al. 2013).

[explain overall picture, $\tau_{\rm d}$ vs. $\tau_{\rm cl}$]

2.1 Cosmic ray transport

As previously noted, secondaries produced by shock accelerated CRp have the wrong spatial profile to explain RH observations; because they arise from a two body process, they are too centrally concentrated. They also produce γ-ray emission in excess of Fermi-LAT upper limits (Arlen et al. 2012; Brunetti et al. 2012; Ackermann et al. 2014). However, if CRps stream in the ICM, then their spatial profile could potentially flatten sufficiently (Enßlin et al. 2011; Wiener et al. 2013). This scenario is very attractive: it generates seed electrons with the right spatial footprint, and by removing CRps from the core, obeys gamma-ray constraints. Turbulence plays two opposing roles: Alfvénic turbulence damps waves generated by the CR streaming instability (Yan & Lazarian 2002; Farmer & Goldreich 2004), thus reducing self-confinement; but compressible fast modes scatter CRs directly. Turbulent damping is still efficient for highly subsonic conditions (Wiener et al. 2013), while we assume compressible fast modes to only provide effective spatial confinement during the periods of transonic, highly super-Alfvénic ($M_{\rm A}\sim 5$) turbulence associated with mergers. Thus, CRs can stream out when the cluster is kinematically quiescent. Furthermore, even Alfvénic streaming timescales are relatively short ($\sim 0.1-0.5$ Gyr; Wiener et al. 2013) compared to the timescale on which the CRp population is built up. Based on these findings, we adopt a toy model for our *M-streaming* scenario in which CR streaming instantaneously produces flat CRp profiles. ~~We assume that CRs cannot stream significantly past perpendicular *B*-fields at the accretion shock, so that the total number of CRs is conserved within the galaxy cluster during the streaming process.~~

Given a seed population of CRs, we adopt essentially the same set of plasma physics assumptions as the reacceleration model for RHs (Brunetti & Lazarian 2007, 2011). We solve the isotropic, gyro-phase averaged Fokker-Planck equation (via a Crank-Nicholson scheme) for the time evolution of the CRe distribution in the Lagrangian frame (Brunetti & Lazarian 2007, 2011):

$$\begin{aligned}\frac{df_{\rm e}(p,t)}{dt} &= \frac{\partial}{\partial p}\left\{f_{\rm e}(p,t)\left[\left|\frac{dp}{dt}\right|_{\rm coul}+\frac{p}{3}\left(\boldsymbol{\nabla}\cdot\boldsymbol{v}\right)+\left|\frac{dp}{dt}\right|_{\rm r}\right.\right.\\ &\left.\left.-\frac{1}{p^2}\frac{\partial}{\partial p}\left(p^2 D_{pp}\right)\right]\right\}-\left(\boldsymbol{\nabla}\cdot\boldsymbol{v}\right)f_{\rm e}(p,t)-\boldsymbol{\nabla}\cdot\boldsymbol{F}_{\rm stream}\\ &+\frac{\partial^2}{\partial p^2}\left[D_{pp}f_{\rm e}(p,t)\right]+Q_{\rm e}\left[p,t;f_{\rm p}(p,t)\right]. \qquad (1)\end{aligned}$$

Here $f_{\rm e}$ is the one-dimensional distribution in position x (suppressed for clarity), momentum p and time t (which is normalized such that the number density is given by $n_{\rm e}(t)=\int dp f_{\rm e}(p,t)$), $d/dt=\partial/\partial t+\boldsymbol{v}\cdot\boldsymbol{\nabla}$ is the Lagrangian derivative, $\boldsymbol{v}$ is the gas velocity, $|dp/dt|$ represents radiative (r) and Coulomb (coul) losses, D_{pp} is the momentum space diffusion coefficient, and $Q_{\rm e}$ denotes the injection rate of primary and secondary electrons in the ICM. The $\boldsymbol{\nabla}\cdot\boldsymbol{v}$ terms represent adiabatic gains and losses and the $\boldsymbol{\nabla}\cdot\boldsymbol{F}_{\rm stream}$ terms represent super-Alfvénic CR streaming. For details about $F_{\rm stream}$ please see Wiener et al. (2013). During post-processing of our Coma-like cluster simulation, we solve the Fokker-Planck equation over a redshift interval from $z=5$ to 0. The simulated cluster undergoes a major merger over the last 1-2 Gyrs that is thought to inject large turbulent eddies. Following Brunetti & Lazarian (2007, 2011) (see also Yan & Lazarian 2004; Miniati 2015) we assume that about one Gyr after core passage the fields have decayed down to the smallest scales where reacceleration is most efficient ($D_{pp}\sim k_{\rm cut}$) and the radio halo turns on shortly after. Note that the exact decay time of the turbulens is of minor importance, since the thermal and CR quantities are very similar a few 100 Myrs before and after $z=0$ where we have chosen to evaluate the simulations. This delay naturally explains why giant radio halos are only seen in a fraction of all merging clusters. In all our calculations we assume that turbulent reacceleration efficiently accelerates particles for $\tau_{\rm cl}\sim 650$ Myrs (which is roughly the cascade time on which turbulence is damped) and that during this turbulent phase CR streaming and spatial diffusion can be neglected. In our *M-streaming* model, CR streaming and diffusion are incorporated separately during kinematically quiescent times that precede the merger. As a result, flat CRp profiles are produced on relatively short timescales ($\sim 0.1-0.5$ Gyr). This allows us to implicitly solve for CR streaming in our calculations, where we adopt a toy model that enforce a flat CRp profile at all quiescent times (Wiener et al. 2013). We assume that CRs cannot stream significantly past perpendicular *B*-fields at the accretion shock, so that the total number of CRs is conserved within the virial radius during the streaming process. Finally, since streaming is much more efficient for the CRps, we can ignore this effect for the CRes.

The time evolution of the spectral energy distribution of CRps, $f_{\rm p}$, is similarly given by:

$$\begin{aligned}\frac{df_{\rm p}(p,t)}{dt} &= \frac{\partial}{\partial p}\left\{f_{\rm p}(p,t)\left[\left|\frac{dp}{dt}\right|_{\rm C}+\frac{p}{3}\left(\boldsymbol{\nabla}\cdot\boldsymbol{v}\right)\right.\right.\\ &\left.\left.-\frac{1}{p^2}\frac{\partial}{\partial p}\left(p^2 D_{pp}\right)\right]\right\}-\left(\boldsymbol{\nabla}\cdot\boldsymbol{v}\right)f_{\rm p}(p,t)-\boldsymbol{\nabla}\cdot\boldsymbol{F}_{\rm stream}\\ &+\frac{\partial^2}{\partial p^2}\left[D_{pp}f_{\rm p}(p,t)\right]-\frac{f_{\rm p}(p,t)}{\tau_{\rm had}(p)}+Q_{\rm p}(p,t), \qquad (2)\end{aligned}$$

where $Q_{\rm p}(p,t)$ denotes the injection rate of shock accelerated CRps as a function of momentum p and time t, and $\tau_{\rm had}$ is the timescale of hadronic losses that produce pions via CRp collisions with thermal protons of the ICM (e.g. Brunetti & Lazarian 2011).

2.2 Turbulent reacceleration

We incorporate momentum diffusion for electrons and protons from transit-time-damping (TTD) resonance with compressible MHD turbulence, to model Fermi-II reacceleration (Brunetti & Lazarian 2007, 2011). The TTD resonance requires the wave frequency $\omega = k_\parallel v_\parallel$, where $k_\parallel$ and $v_\parallel$ are the parallel (projected along the magnetic field) wavenumber and particle velocity, respectively. This implies that the particle transit time across the confining wave region matches the wave period, $\lambda_\parallel/v_\parallel = T$. Note, the CRs' gyroradius does not enter the resonance condition. Hence the CRs that are in resonance with compressible waves experience Fermi-II acceleration irrespectively of the length scale of the perturbation.

However, the resonance changes the component of particle momentum parallel to seed magnetic fields, which over time leads to increasing anisotropy in the particle distribution that decreases the efficiency of reacceleration with time. As in Brunetti & Lazarian (2011), we assume that there exists a mechanism—such as the firehose instability—that isotropizes the CR distribution function at the gyroscale and on the reacceleration time scale, which ensures sustained efficient reacceleration with time. The particle pitch-angle averaged momentum-diffusion coefficient of isotropic particles that couple to fast magnetosonic modes via TTD resonance is (Brunetti & Lazarian 2007, Eqn. 47):

$$D_{pp}(p,t) = \frac{\pi}{16}\frac{p^2}{c\,\rho}\left\langle\frac{\beta|B_k|^2}{16\pi\,W}\right\rangle I_\theta \int_{k_{\rm cut}} \mathcal{W}(k) k\,dk\,, \tag{3}$$

where β is the thermal-to-magnetic pressure ratio, and c is the speed of light. The energy density W of a mode in a magnetized plasma stems from both electromagnetic fields and resonant particles. For a high-β plasma, the pitch angle averaged ratio of beta-weighted magnetic-to-total energy density saturates to $\langle\beta|B_k|^2/2W\rangle \approx 10^{1.4}$ (see Figure 2 in Brunetti & Lazarian 2007). The pitch angle of the CR momentum with the magnetic field orientation is given by θ, and

$$I_\theta = \int_0^{\arccos(V_{\rm ph}/c)} d\theta \frac{\sin^3\theta}{|\cos\theta|}\left[1+\left(\frac{V_{\rm ph}}{c\,\cos\theta}\right)^2\right]^2. \tag{4}$$

Here $V_{\rm ph}$ is the phase velocity of the fast magnetosonic waves given approximately by the sound speed, $V_{\rm ph} \sim c_{\rm s}$. For a sound speed typical for the ICM of 1000 km/s, $I_\theta \approx 5$. As in Brunetti & Lazarian (2007), we initially assume that the velocity of turbulent eddies is $V_0 \approx 0.47 c_{\rm s}$ throughout the cluster. This gives a turbulent acceleration time scale, $\tau_D = p^2/4D_{pp}$, that is typically few 100 Myrs in the ICM (see Tab. 1 for more details).

We focus on a scenario where the turbulence is injected at the largest scale that is driven by the merging cluster and accreting matter. The diffusion equation for isotropic MHD turbulence in k–space is given by

$$\frac{\partial \mathcal{W}(k,t)}{\partial t} = \frac{\partial}{\partial k}\left[k^2 D_{kk}\frac{\partial}{\partial k}\left(\frac{\mathcal{W}(k,t)}{k^2}\right)\right] - \sum_i \Gamma_i(k,t)\mathcal{W}(k,t) + I(k,t) \tag{5}$$

where we assume that the volumetric injection rate of turbulence $I(k,t)$ is constant over time with a fixed rate I_0 so that $I(k,t) \equiv I(k) = I_0\,\delta(k-k_o)$. The different damping terms are given by $\Gamma_i(k,t)$ and D_{kk} is the wave–wave diffusion coefficient of magnetosonic waves in the k–space represented by

$$D_{kk} \approx V_{\rm ph} k^4 \left(\frac{\mathcal{W}(k)}{\rho\, V_{\rm ph}^2}\right). \tag{6}$$

We adopt a simplified isotropic MHD turbulent spectrum based on Kraichnan's picture for the fast modes per elemental range dk of the form

$$\mathcal{W}(k) = \sqrt{2/7\, I_0\, \rho\, \langle V_{\rm ph}\rangle}\, k^{-3/2}, \tag{7}$$

for $k_0 < k < k_{\rm cut}$. Here we adopt a injection scale of the turbulence, $k_0 = 2\pi/(100$ kpc), that is in line with previous work (Brunetti & Lazarian 2007, 2011) **AP: need to be motivated beter? why not 1 Mpc** The profile of injected turbulence is also highly uncertain, however we assume it correlates to the thermal energy density to some power of the merging clusters. Hence we assume volumetric injection rate of turbulent energy, $I_0 \propto \epsilon_{\rm th}^{\alpha_{\rm tu}}$, and determine the normalization by requiring that the turbulent energy in compressible modes $E_{\rm turb} = \int\int \mathcal{W}(k)\mathrm{d}k\mathrm{d}V = X_{\rm tu} E_{\rm th}$, where $E_{\rm th}$ is the total thermal energy. We adopt a turbulent energy ratio[1] $X_{\rm tu} = 0.2$ within the radio halo. In this work we investigate different spatial models for injected turbulence. With the above choice of normalization, the turbulent energy density becomes $\epsilon_{\rm turb} \propto \epsilon_{\rm th}^{(\alpha_{\rm tu}+1)/2}/T^{1/4}$, where T is the temperature of the gas, $\alpha_{\rm tu} = 0.67$ for *M-turbulence*, $\alpha_{\rm tu} = 0.82$ for *M-streaming*, and $\alpha_{\rm tu} = 0.88$ for *M-primaries* (see Figure 2 for visualisation). Note that in previous work on the Coma cluster, $\epsilon_{\rm turb} \propto \epsilon_{\rm th}$ was adopted which roughly corresponds to $\alpha_{\rm tu} = 1$ (Brunetti et al. 2012) and together with the different distributions for seed CRes constitute the main differences compared to our work. Our flatter turbulent profiles are motivated by fits to cosmological simulations (Lau et al. 2009; Shaw et al. 2010; Vazza et al. 2011; Battaglia et al. 2012) and the range indicates uncertainties of the turbulent profile in Coma. Future observations (by Astro-H) and simulations will help to clarify this issue. Provided dissipation of turbulence in the ICM is collisionless, turbulent cascades of compressible modes become suppressed when thermal and relativistic particles resonantly interact with magnetosonic waves via TTD on a timescale Γ^{-1} that approaches the cascading timescale given by $\tau_{kk} \approx k^2/D_{kk}$. Thus, the cascade is suppressed for wave numbers above

$$k_{\rm cut} \approx \frac{81}{14}\frac{I_0}{\rho\langle V_{\rm ph}\rangle}\left(\frac{\langle\sum_i \Gamma_i(k,\theta)\rangle}{k}\right)^{-2}, \tag{8}$$

where $2\pi/k_{\rm cut} \sim 0.1-1$ kpc in the ICM. This constitutes an effective mean free path for CRs, unless plasma instabilities can mediate interactions between turbulence and particles on smaller scales (Brunetti & Lazarian 2011). In this work we only consider damping of the turbulence via TTD due to thermal electrons, and neglect subdominant damping with thermal protons and relativistic particles (conversely, the turbulence has important effects on the reacceleration of CRs). The latter will be subdominant in the ICM for a CR-to-thermal energy density ratio $\lesssim 10\%$ (Brunetti & Lazarian

[1] Simulations show that the compressible modes contribute a factor 0.2 – 0.4 to the total turbulent energy (Beresnyak et al. 2013; Miniati 2015). Furthermore, the total turbulent energy is typically $\sim 15-70\%$ of the thermal energy in a cluster Vazza et al. (2011) which is in agreement with our adopted value of $X_{\rm tu}$.

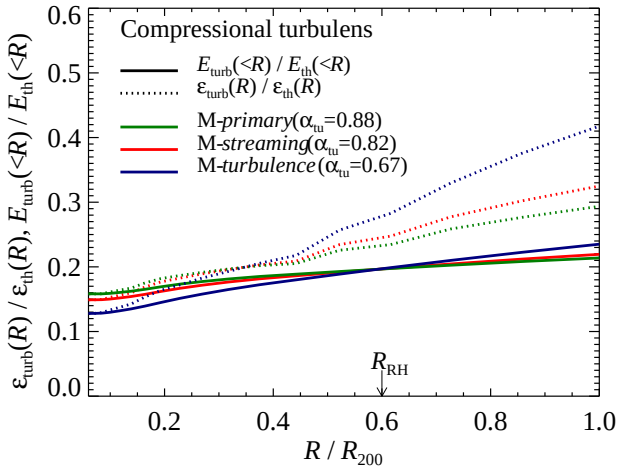

Figure 2. The ratio of turbulent-to-thermal energy densities (solid lines) and cumulative energies (dotted lines) in our three models. The energy densities are parametrized as $\epsilon_{turb} \propto \epsilon_{th}^{(\alpha_{tu}+1)/2}/T^{1/4}$ and normalized such that the total turbulent energy in compressible modes E_{turb} for each scenario makes up about 20% of the total thermal energy E_{th} inside the radio halo ($R_{RH} \approx 0.6R_{200}$). The turbulent profiles explore the uncertainty in the cluster turbulence and are motivated by the cosmological simulation in (Lau et al. 2009; Shaw et al. 2010; Vazza et al. 2011).

2007), which is always satisfied in our models. The azimuthally averaged turbulent damping rate from thermal electrons (Brunetti & Lazarian 2007) in a high-β plasma is

$$\langle \Gamma_e \rangle \approx \langle k\, V_{ph}\, \sqrt{3\pi x/20}\exp(-5x/3)\sin^2\theta \rangle \approx 0.0435 k\, V_{ph}, \quad (9)$$

where $x = (m_e/m_p)/\cos^2\theta$. To compute the synchrotron surface brightness profiles, we use the profile of the magnetic field strengths derived from Faraday rotation observations of Coma (Bonafede et al. 2010) in combination with the density profile derived from X-ray measurements (Briel et al. 1992).

For reference we show in Table 1 both the thermal quantities and the timescales for CR cooling and (re)acceleration for three different spatial regions of the RH. Interestingly the reacceleration timescale τ_D is similar between our three models, where the difference comes from turbulent profile parameterized with α_{tu}. This implies that even small differences in the turbulent profile could impact the seed CRs significantly.

2.3 Spherically symmetric models

In this section we develope a simple framework that will be used to test the robustness of our models to the critical parameters for CRs and turbulence in section 3. Here we do not follow single Lagrangian particles in the cluster, instead we use a more simple approach where we solve the Fokker-Plack equation in static spherical shells for injection, reacceleration, and losses of the CRs. Once the CRs have been reaccelerated for $\tau_{cl} = 650$ Myr, we calculate the radio emission and compare the profile and spectra for different parametrizations.

We adopt both the density Briel et al. (1992) and temperature Bonamente et al. (2009); Arnaud et al. (2001) profiles derived from X-ray observations of the Coma cluster. They are given by:

$$n_e = \frac{3.4\times10^{-3}}{\left[1+(R/294\,\mathrm{kpc})^2\right]^{1.125}}$$
$$Tk_B = 8.25\,\mathrm{keV}\left[1+(R/0.5R_{200})^2\right]^{-0.32}. \quad (10)$$

The virial radius of Coma is given by $R_{200} = 2300$ kpc. The bulk of the CRps are injected by relatively low Mach number shocks and parametrized by $f_{CRp,inj}(p) = C_{CRp,inj}\, p^{-2.5}$. The CRps trace the thermal gas with $C_{CRp,inj} \propto \epsilon_{th}^{\alpha_{CR,spat}}$, where the normalization is fixed by assuming that the injected CR energy in the last 650 Myrs make up 0.03% of the thermal energy inside the virial radius, i.e. $\int_0^{R_{200}} \epsilon_{CRp,inj} dV / \int_0^{R_{200}} \epsilon_{th} dV = 0.0003$. The spectrum of the initial CRp distibtion is determined by the steady state between injection and cooling,

$$f_{CRp,0} \approx \frac{\int_p^\infty f_{CRp,inj}(p')dp'}{\left|\frac{dp}{dt}\right|_{coul} + \frac{p}{\tau_{had}}}, \quad (11)$$

where the normalization is fixed by $\int_0^{R_{200}} \epsilon_{CRp,inj} dV / \int_0^{R_{200}} \epsilon_{th} dV = 0.003$. Similarly, the initial CRe distribution is given by the steady state between cooling (Coulomb, invers Compton, and synchroton) and injection of secondary CRes from $f_{CRp,0}$. We also include the contineous injection of secondary CRes during τ_{cl}. The compressible turbulence responsible for reacceleating both the CRps and CRes is parametrized by $I_0 \propto X_{tu}(n_e T)^{\alpha_{tu}}$. The diffusion constant D_{pp} is calculated for each radial bin using Eqns. 3-9. All parameters and assumptions are similar to what is used for our simulated cluster.

Table 1. Thermal quantities and timescales for different spatial regions in a Coma like cluster.

	spatial regions		
	$0.1\,R_{RH}^{(2)}$	$0.3\,R_{RH}^{(2)}$	$R_{RH}^{(2)}$
thermal quantities[1]			
ρ [10^{-27} g cm^{-3}]	3.0	1.6	0.15
T [10^8 K]	1.4	1.0	0.58
timescales[1]			
$\tau_D(M\text{-}primaries)$[3] [Gyr]	0.45	0.44	0.39
$\tau_D(M\text{-}streaming)$[3] [Gyr]	0.50	0.47	0.34
$\tau_D(M\text{-}turbulence)$[3] [Gyr]	0.69	0.56	0.27
$\tau_{IC/sync}(P = 10^4 m_e c)$[4] [Gyr]	0.11	0.15	0.22
$\tau_{had}(P = 100 m_p c)$[5] [Gyr]	2.4	4.5	47
$\tau_{coul}(P = m_e c)$[6] [Gyr]	0.0092	0.017	0.17

Notes:
(1) Median quantities from our simulated post-merging cluster g72a.
(2) Radius of the giant radio halo in Coma where $R_{RH} \approx 0.6\,R_{200}$.
(3) Fermi-II reacceleration for both electrons and protons at all energies.
(4) Inverse Compton and synchrotron cooling for electrons.
(5) Catastrophic losses for protons.
(6) Coulomb cooling for electrons (protons factor m_e/m_p smaller).

2.4 Cosmological simulation methodology

In this paper we focus on our simulated cluster, g72a, which is a massive $1.6\times10^{15}\,M_\odot$ cluster that experienced a merger

about 1-2 Gyrs ago (Dolag et al. 2009). Since the cluster mass, density and temperature profiles are all similar to the well studied Coma cluster (Pfrommer et al. 2007; Pinzke & Pfrommer 2010), we will compare our calculations to radio and gamma-ray observations of Coma.

We use a simple test-particle model for the CR acceleration and injection, where each shock inject CRs that trace a power-law in momentum,

$$f(p,t) = C(t)\, p^{\alpha_{\rm inj}}\,, \tag{12}$$

determined by the normalization $C(t)$ and the spectral index $\alpha_{\rm inj} = \frac{(\gamma_{\rm ad}+1)\mathcal{M}^2}{(\gamma_{\rm ad}-1)\mathcal{M}^2+2}$ that depends on the adiabatic index $\gamma_{\rm ad} = 5/3$ and the Mach number of the shock $\mathcal{M}$. It is given by the ratio of the upstream velocity (u_2) and the sound speed (c_s). The CR number density and CR energy density are derived from $n_{\rm CR} = \int_{p_{\rm inj}}^{\infty} {\rm d}p\, f(p)$ and $\epsilon_{\rm CR} = \int_{p_{\rm inj}}^{\infty} {\rm d}p\, f(p)\, T(p)$, respectively, where $T(p) = (\sqrt{1+p^2}-1)\, m\, c^2$ is the kinetic energy of a particle with momentum p. We adopt a fit to Monte Carlo simulations of the thermal leakage process that relates the momentum of injected protons ($p_{\rm inj}$) to the thermal energy ($p_{\rm th}$) of the shocked plasma (Kang & Ryu 2011):

$$\begin{aligned} p_{\rm inj} &= x_{\rm inj} p_{\rm th} = x_{\rm inj}\sqrt{\frac{2\,kT_2}{mc^2}}\,, \\ \text{where}\quad x_{\rm inj} &\approx 1.17\frac{u_2}{p_{th}\,c}\left(1+\frac{1.07}{\epsilon_B}\right)\left(\frac{\mathcal{M}}{3}\right)^{0.1}. \end{aligned} \tag{13}$$

Here $\epsilon_{\rm B} = B_0/B_\perp$, B_0 is the amplitude of the downstream MHD wave turbulence, and $B_\perp$ is the magnetic field along the shock normal. The physical range of $\epsilon_{\rm B}$ is quite uncertain due to complex plasma interactions. In this paper, we adopt $\epsilon_{\rm B} = 0.23$, which we will later see corresponds to a conservative maximum energy acceleration efficiency for protons of 10%. To derive the acceleration efficiency, $\zeta_{\rm inj}$, we first have to infer the particle injection efficiency, which is the fraction of downstream thermal gas particles which experience diffusive shock acceleration (for details see Pinzke et al. 2013),

$$\eta_{\rm CR,lin} = \frac{4}{\sqrt{\pi}}\,\frac{x_{\rm inj}^3}{\alpha_{\rm inj}-1}\,{\rm e}^{-x_{\rm inj}^2}. \tag{14}$$

The particle injection efficiency is a strong function of $x_{\rm inj}$ that depends on both $\mathcal{M}$ and $\epsilon_{\rm B}$. The energy density of CRs that are injected and accelerated at the shock (neglecting the CR back reaction on the shock) is given by

$$\Delta\epsilon_{\rm CR,lin} = \eta_{\rm CR,lin}(\mathcal{M})\, T_{\rm CR}(\mathcal{M}, p_{\rm inj})\, n_{\rm th}(T_2), \tag{15}$$

and the CR energy injection and acceleration efficiency is:

$$\zeta_{\rm lin} = \frac{\Delta\epsilon_{\rm CR,lin}}{\Delta\epsilon_{\rm diss}}, \quad \text{where} \quad \Delta\epsilon_{\rm diss} = \epsilon_{\rm th2} - \epsilon_{\rm th0}\left(\frac{\rho_2}{\rho_0}\right)^{\gamma_{\rm ad}}. \tag{16}$$

The dissipated energy density in the downstream regime, $\Delta\epsilon_{\rm diss}$, is given by the difference of the thermal energy densities in the pre- and post-shock regimes, corrected for the adiabatic energy increase due to gas compression.

We limit the acceleration efficiency to $\zeta_{\rm max}$ by steepening the spectral index of the injected population $\alpha_{\rm inj}$ to $\alpha_{\rm sub}$ so that $\zeta_{\rm lin} \leq \zeta_{\rm max}$ is always fulfilled. The slope $\alpha_{\rm inj}$ impact $\zeta_{\rm inj}$ via the mean energy per particle given by $T_{\rm CR} = \epsilon_{\rm CR}/n_{\rm CR}$. This procedure conserves energy and is motivated by models of non-linear shock acceleration where a sub-shock with a lower compression ratio (and hence steeper spectral index) forms (e.g., Ellison et al. 2000). Given our assumed $\epsilon_{\rm B} = 0.23$, we find that for strong shocks where $\alpha \lesssim 2.3$ the spectral slope is steepened by a maximum of ~ 10 per cent in low temperature regimes ($kT \sim 0.1$ keV), while the steepening is much smaller for high temperature regimes ($kT \sim 10$ keV) that are more relevant for clusters. Since $p_{\rm inj}$ remains fixed, so does the CR number density $n_{\rm CR}$. Hence we can solve for the renormalized normalization constant $C_{\rm sub}$ using $n_{\rm CR}$ and Eqn. 14:

$$C_{\rm sub} = \eta_{\rm CR,lin}\,(\alpha_{\rm sub}-1)\, p_{\rm inj}^{\alpha_{\rm sub}-1}\,, \tag{17}$$

where the new distribution function is given by $f(p,t) = C_{\rm sub} p^{-\alpha_{\rm sub}}$. We set an upper limit on the ratio of accelerated proton-to-dissipated energy in the downstream of strong shocks that varies from $\zeta_{\rm max} \sim 1-10\%$, depending on the adopted model (for more details, see Section 4).

In our Galaxy, the CRe-to-CRp ratio at a few GeV is $K_{\rm ep} \sim 10^{-2}$. Hence, we adopt this as a fiducial value for the CRe-to-CRp acceleration efficiency (see Pinzke et al. (2013) for more discussion). However, as recent PIC simulations have shown, this is likely very different at weak shocks, with electrons efficiently accelerated at perpendicular shocks (Guo et al. 2014a,b), and ions efficiently accelerated at parallel shocks (Caprioli & Spitkovsky 2014). Thus, depending on magnetic geometry, $K_{\rm ep}$ could be either larger or smaller. Some observations of radio relics suggest high values of $K_{\rm ep}$, due to the absence of gamma-ray emission, which probes the CRp population (Vazza & Brüggen 2014). This suggests primary CRes as a viable alternative scenario to secondary CRes as seeds for the giant RHs. In our *M-primaries* scenario, the injected distribution of CRes is derived in the same way as for the CRps. Once they have been accelerated to relativistic energies, injected electrons and protons are indistinguishable. We therefore assume that CRp and CRe have the same distribution function $f_{\rm CRe}(p) = K_{\rm ep} f_{\rm CRp}(p)$, with a different normalization (due to differing acceleration efficiencies) $K_{\rm ep} = 0.1$ (which is viable for primarily perpendicular shocks Guo et al. 2014a). While this appears to contradict the radial bias of magnetic fields in the bulk of the ICM as suggested by observations (Pfrommer & Dursi 2010) and cluster simulations (Ruszkowski et al. 2011), it does not necessarily apply to the accretion shock regions, which show a field geometry with a net perpendicular bias with respect to the shock normal—at least for giant radio relics (van Weeren et al. 2010).

3 PARAMETER SPACE EXPLORATION WITH SPHERICAL MODELS

In this section we explore the robustness of our models to crucial parameters. Figure 3 shows how assumptions about turbulence and CRs impact the radio emission. We find that the level of turbulence has a large impact on both radio spectra and profile, while the parameter $\alpha_{\rm tu}$ that determines the spatial profile of turbulence mainly influence the radio profiles. Interestingly, assumptions about CRs have less impact on radio emission. This can be understood by looking at the scaling of parameters to the reacceleration timescale, where $\tau_{\rm D} \propto X_{\rm tu}^2$. The CRps approximately gain a factor $\Delta C_{\rm reacc.} \sim \exp\left[\frac{(2+\alpha)(1-\alpha)}{4}\frac{\tau_{\rm cl}}{\tau_{\rm D}}\right]$ during reacceleration if injection and cooling are neglected. The CRes gain a similar factor from reacceleration, however in the region around $0.1\,R_{200}$ the

Coulomb cooling timescale ($\tau_{\rm coul} \approx 0.01\,{\rm Gyr}$) is much shorter than $\tau_{\rm D} \approx 0.5\,{\rm Gyr}$, hence $\Delta C_{\rm reacc.}$ will be greatly reduced for the electrons. The spatial region is important when we derive the radio spectrum, since in order to compare to observations we integrate the CR profile out to $\sim 0.2\,R_{200}$. For a CRp spectral index $\alpha_{\rm CR} \sim 2.5$, $\Delta C_{\rm reacc.} \sim \exp\left[1.7\frac{\tau_{\rm cl}}{\tau_{\rm D}}\right] \sim 10$ for $X_{\rm tu} = 0.2$ and $\alpha_{\rm tu} = 0.8$. This is confirmed by the top panels in Fig. 3. Increasing from $X_{\rm tu} = 0.2$ to $X_{\rm tu} = 0.3$, gives us a $\Delta C_{\rm reacc.} \sim 100$, which is roughly confirmed by same figures. The factor 2-3 difference in the figure is due to the shorter reacceleration timescale that increase the contribution from reaccelerated CRes. Hence we conclude that the radio emission is much more sensitive to the exponential dependence on turbulence than the linjear dependence on injected CRs. **AP: Too complicated, perhaps cut or simplify?**

4 RESULTS OF COSMOLOGICAL SIMULATIONS

In this section we show that our three models individually reproduce the observed Coma radio halo without violating gamma-ray bounds. The level of emission is mainly driven by how efficient the CRs are reaccelerated and for how long. After turbulent reacceleration, the volume-weighted, relative CRp energy density and relative CRp number density inside the RH for *M-turbulence* (*M-streaming*), are found to be 2 (3) % and 2×10^{-8} (5×10^{-8}), respectively. As we will see later, these densities are just of the right order of magnitude to reproduce radio observations in the Coma cluster.

AP: move to a scaling subsection? The diffusion constant, $D_{\rm pp} \propto I_0/\rho c_s \propto X_{\rm tu}^2 k_0 \epsilon_{\rm th}^{\alpha_{\rm tu}-1}\sqrt{T}$, where we adopt the same level of compressible turbulence, $X_{\rm tu} = 0.2$, for all models. The reaccelerated CRs are exponentially dependent on this parameter as long as $\tau_D > \tau_{\rm cl}$, where $\tau_{\rm cl}$ represent the duration of reacceleration of the merger which we assume to be 650 Myrs long. Note that a fixed reacceleration timescale $\tau_D \sim 1/D_{\rm pp} \sim 0.2 - 0.7\,{\rm Gyr}$ is required to explain the observations for each model and radial bin. This allows us to interchange $\tau_{\rm cl} \propto X_{\rm tu}^2 \propto k_0$, i.e. a longer reacceleration duration have to be compensated by lowering the level of turbulence or increasing the injection scale of turbulence to keep τ_D constant. We also exploit the large uncertainty in the turbulent profile and adjust $\alpha_{\rm tu}$ for each model so that the CRs have the correct spatial profile to match the radio emission. The shape of the spectrum for each of model is more complicated and is determined both from reacceleration and as well as the gains and losses during the formation of the cluster. It depends only weakly on the specifics of the CR injection at the shocks (where the Mach number distribution of the shocks is the most important quantity). The normalization of the spectrum is mainly determined from the maximum acceleration efficiency (together with the uncertain parameters $X_{\rm tu}$, $\tau_{\rm cl}$, and k_0). Given the freedom in the turbulens, it might not be surprising that we match the radio profile in Coma. Although, matching the spectrum without violating gamma-ray bounds for each of our three models is more surprising and is not a consequence of parameter fitting. We believe that it is ultimately a consequence of the adopted physics and hint that reacceleration is a viable explanation for giant radio halos. Below we discuss in more detail the different emission components of Coma.

4.1 Radio profile

In Fig. 4, we find that all three scenarios in which the seeds undergo Fermi-II reacceleration can reproduce the Coma RH profile at 352 MHz. In the panel *Brunetti et al. (2012)* we show that without CR streaming or a flat turbulent profile, our simulations of reaccelerated CRs produce radio profiles that are too steep. Indeed, even using the assumptions of previous work – where complete freedom in the seed population was allowed – it is not possible to reproduce observations in both frequencies in any model. Note that decreasing acceleration efficiency with radius does not change this conclusion much because of the weak radial dependence of $D_{\rm pp}(R) \propto \epsilon_{\rm th}(R)^{\alpha_{\rm tu}-1}\sqrt{T(R)}$. This signals that the problem is generic and requires either additional modifications to the plasma physics of acceleration or a better understanding of potential observational systematics. In addition there are differences in the simulated density and temperature profiles in comparison to the observed profile in Coma that impact the CR abundance as well as cooling and reacceleration.

In principle, reacceleration via TTD leads to spectral steepening with particle energy due to the inefficiency of the acceleration process to counter the stronger cooling losses with increasing energy. Since synchrotron emission peaks at frequency $\nu_{\rm syn} \simeq 1\,B/\mu{\rm G}(\gamma/10^4)^2\,{\rm GHz}$, this translates into a spectral steepening of the radio spectrum (see Fig. 5). A given radio window samples higher energy electrons for a decreasing field strength in the cluster outskirts. Hence, the spectral steepening with energy should translate into a radial spectral steepening (Brunetti et al. 2012). However, because of the weak dependence of the electron Lorentz factor on emission frequency ($\gamma \propto \sqrt{\nu_{\rm syn}}$), this effect is only visible in our simulations for $\nu_{\rm syn} \gtrsim 5$ GHz. Most importantly, our simulated fluid elements at a given radius sample a broad distribution of shock history, density and temperature, which implies very similar synchrotron brightness profiles at $\nu_{\rm syn} = 352$ MHz and 1.4 GHz. The discrepancy of the observed and simulated 1.4 GHz profiles could instead be due to systematic flux calibration error in single dish observations. These could arise, for instance, due to errors in point source subtraction. Interestingly, we can match the 1.4 GHz data if we reduce the zero point by adding 10% of the central flux to every data point; this flattens the outer profile[2]. Alternatively, this may point to weaknesses in the theoretical modeling of the particle acceleration process and may require a stronger cutoff in the particle energy spectrum.

4.2 Radio spectrum

In Fig. 5 we show that our three models that include Fermi-II reacceleration can individually reproduce the convexly curved total radio spectrum found in the Coma cluster. Seed CRs in *M-streaming* and *M-turbulence* that do not experience turbulent reacceleration have a power-law spectrum in disagreement with observations. In order to match both the spatial and spectral profiles in Coma, we adopt an acceleration efficiency for the strongest shocks in our three models *M-primaries*, *M-streaming*, and *M-turbulence* to $\zeta_{\rm e} < 0.003$, $\zeta_{\rm p} < 0.1$, and $\zeta_{\rm p} < 0.03$, respectively. Following the Mach

[2] Lawrence Rudnick, private communication.

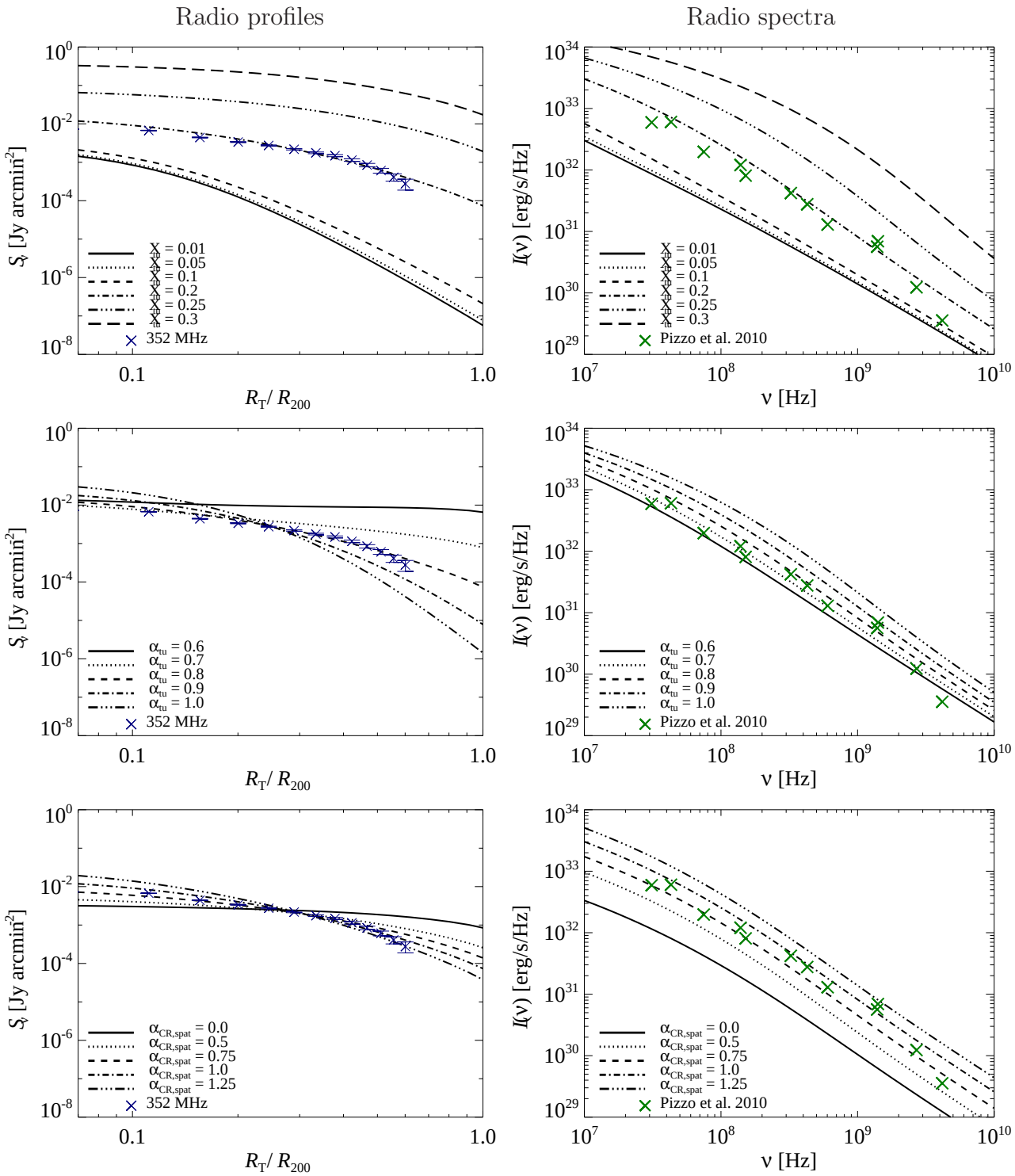

Figure 3. Sensitivity of radio emission in Coma cluster to critical parameters. *Left panels* show the radio surface brightness profiles. We compare profiles at 352 MHz (blue lines and crosses, Brown & Rudnick 2011) to predicted emission from Fermi-II reaccelerated CR electrons populations (black lines). *Right panels* show radio synchrotron spectra. The green crosses are compiled from observations Pizzo (2010), while the black lines show predicted emission from reaccelerated CR electrons. The upper panels show the sensitivity to the level of turbulence ($X_{\rm tu}$), middle panels show the impact of different turbulent profiles ($\alpha_{\rm tu}$), and lower panels show the dependence on spatial distributions of initial and injected CRs ($\alpha_{\rm CR,spat}$). We adopt the following fiducial values for parameters that are not varied in each panel: $X_{\rm tu}$ = 0.2, $\alpha_{\rm tu}$ = 0.8, and $\alpha_{\rm CR,spat}$ = 1.0. Note that the radio emission is much more sensitive to assumptions about turbulent parameters than CRs.

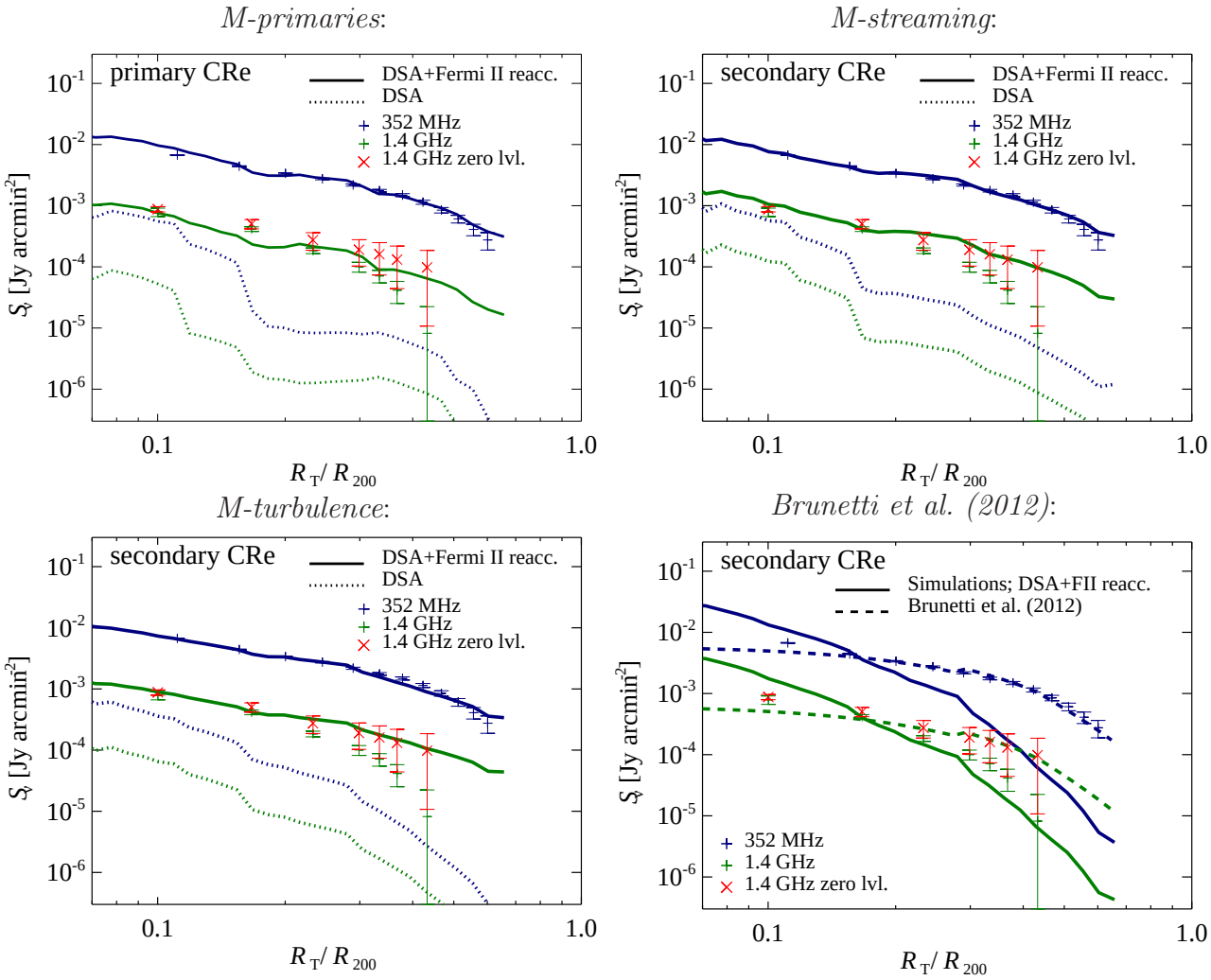

Figure 4. Radio surface brightness profiles of Fermi-II reaccelerated CR electrons of a simulated post-merging cluster similar to Coma. We compare profiles at 352 MHz (blue lines and crosses, Brown & Rudnick 2011) to those at 1.4 GHz (green lines and crosses, Deiss et al. 1997). The red crosses show the reprocessed 1.4 GHz data, where a zero level of about 10 % of the central value is adopted. The solid lines show predicted emission from a reaccelerated fossil population, while dotted lines show emission from a fossil population without reacceleration. The panels show the emission of our models *M-primaries* (upper left panel), *M-streaming* (upper right panel), *M-turbulence* (lower left panel), and simulated secondary electrons together with previous estimates (Brunetti et al. 2012) for the Coma cluster (lower right panel).

number ($\mathcal{M}$)-dependence of the acceleration efficiency suggested in Pinzke et al. (2013), the efficiency in weak shocks ($\mathcal{M} \sim 2.5-3.5$) that dominates the CR distribution function, has an acceleration efficiency for protons $\zeta_p \sim 0.0001 - 0.01$, and for electrons $\zeta_e \sim 0.001$. Interestingly, we find that the radio luminosity from clusters in the OFF-state (DSA only) and ON-state (DSA and reacceleration) differ by about a factor 10 in all our three models. However, note that for *M-primaries*, the primary CRes that generate most of the radio emission from the cluster in the OFF-state are dominated by only a small fraction of the CRes. These electrons are injected very recently and have not had time to cool yet. Hence we expect there to be a large variance in the OFF-state of different simulated clusters.

While the radio surface brightness has an approximate linear dependence on the acceleration efficiency, it has a strong non-linear dependence on the level of compressible turbulence. Below a critical level ($X_{\rm thres,tu} = \frac{400\,{\rm Myrs}}{\tau_{\rm cl}} X_{\rm tu} \approx 0.12$ in our fiducial model), turbulent reacceleration is negligible, while it rises sharply above this threshold. For instance, for $X_{\rm tu} \gtrsim 0.12$, a factor two change in $X_{\rm tu}$ changes the radio surface brightness by $\sim 10-100$ (see also section 3). In principle this threshold behavior allows us to provide a strict lower bound on turbulence in radio halos. An even more stringent bound on $X_{\rm tu}$ can be inferred from combining radio observations with the gamma-ray observations where the predicted fluxes from both *M-streaming* and *M-turbulence* are close to the upper limits set by Fermi-LAT. If $X_{\rm tu}$ is smaller than in our adopted models (where we assume $X_{\rm tu} = 0.2$), then the efficiency of DSA has to be larger than $\zeta_p \sim 0.1$ for the secondary CRes to reproduce the radio observations. However, since the turbulent reacceleration acts on both the secondary CRes and the CRps, while ζ_p only affects the CRps, these models would produce too much gamma-rays. Hence we conclude that $X_{\rm tu} \gtrsim 0.2$ if all other parameters are kept fixed. Although, we caution the reader to take this limit too

stringent since there are degeneracies between the uncertain parameters $X_{\rm tu} \propto \sqrt{\tau_{\rm D}} \propto \sqrt{k_0}$. We will explore this parameter space further in future work.

4.3 Gamma-rays

The gamma-ray emission from CRps that produce decaying neutral pions could be substantial if the CRps are reaccelerated efficiently enough, hence it is interesting to estimate this emission for our models and compare to upper limits. We predict the gamma-ray emission from *M-turbulence* (*M-streaming*) with $F_\gamma(>500\,\mathrm{MeV}) = 4\times10^{-10}(5\times10^{-10})\,\mathrm{ph\,s^{-1}cm^{-2}}$. The fluxes from these models are slightly larger than in Brunetti et al. (2012), where the differences comes from our steeper CRp profiles in addition to simulation based formalism we rely on that accounts for both Coulomb and hadronic losses during the build up of the CR distribution in contrast to the scaling relations adopted in their paper. Interestingly the gamma-ray flux from both our scenarios are just below recent Fermi-LAT limits derived from a gamma-ray profile similar to *M-turbulence* where $F_\gamma(>500\,\mathrm{MeV}) < 5.3\times10^{-10}\,\mathrm{ph\,s^{-1}cm^{-2}}$ [3] The spectral index of the CRp distribution is relatively steep ($\alpha_{\rm p}\sim2.6$) for the CRp energies $E\gtrsim10$ GeV that are relevant for the injection of radio-emitting secondary CRes. The steep spectrum is ultimately a consequence **AP: of the shock history of the simulated cluster, with a weak dependence on** our test particle model for Fermi-I acceleration (Pinzke et al. 2013), where we steepen the spectral index to avoid acceleration efficiencies above $\zeta_{\rm p}\sim10\%$.

5 CONCLUSIONS

The standard reacceleration model for radio halos (RHs) requires a population of seed electrons to undergo turbulent reacceleration. These seeds are generally thought to be secondary electrons from hadronic cosmic ray proton (CRp) interactions. In this work we use cosmological simulations to derive a population of seed CR protons originating from structure formation shocks and merger shocks during the cluster build up. The resulting secondary population is inconsistent with RH observations. We propose three possible solutions where all reaccelerated CRs produce gamma-ray emission below current upper limits. Additionally, they reproduce both the spectrum and the surface brightness profiles of the Coma radio halo:

(i) **Model *M-primaries*.** If indeed the acceleration efficiency of CRps is below about 0.1 % in weak shocks and the ratio of injected electrons and protons is $K_{\rm ep}\sim10^{-1}$, CR electrons accelerated directly in shocks dominate over secondaries.

(ii) **Model *M-streaming*.** Alternatively, CRps could stream out of the central core and produce flat CR profiles. This seed population of secondary CRes also has the correct spatial and spectral features alone, or potentially complements primaries to explain radio observations.

[3] Fabio Zandanel, private communication. See also Zandanel & Ando (2014); Ackermann et al. (2014). and will be probed in the next few years by Fermi-LAT.

(iii) **Model *M-turbulence*.** Finally, injected turbulence that is flatter than in previously adopted models, which allows seed CRps to follow the steep radial profile that is suggested by structure formation simulations.

Combining radio observations with gamma-ray constraints can be very useful to learn about the plasma of the intracluster medium. Our models (ii) and (iii) relies on CRps to induce secondary CRes that produce the observed radio emission. In addition proton-proton collisions produce neutral pions that decay into gamma rays. Since turbulent reacceleration acts on both CRes and CRps, while the DSA acceleration efficiency (ζ_p) only acts on the CRps, radio observations fix the relation between $X_{\rm tu}$ (the ratio of the total turbulent energy in compressional modes to the total thermal energy) and the acceleration efficiency. With the addition of gamma-ray constraints from Fermi-LAT, we can derive a lower limit to $X_{\rm tu}\gtrsim0.2$ and a upper limit to the acceleration efficiencies of $\zeta_p\lesssim10\%$ ($\zeta_p\lesssim3\%$) for the two models, respectively, for our current choices of other parameters.

How could we distinguish the different possibilities of a dominating primary or secondary seed population of electrons observationally? One possibility that is relative insensitive to adopted parameters in our models is to use high-frequency radio observations (with e.g., the Jansky Very Large Array) where turbulent reacceleration (which has a high energy cutoff) is no longer efficient (see Fig. 5). The negative flux bowl of the Sunyaev-Zel'dovich effect introduces a cutoff of the RH spectrum at frequencies above $\gtrsim$ 10 GHz (Enßlin 2002; Pfrommer & Enßlin 2004b, depending on cluster mass and redshift). Hence the subdominant hadronic radio emission may only be detectable in steep spectrum radio sources (Brunetti et al. 2008), which exhibit a cutoff at lower radio frequencies and are thought to represent dying RHs as a result of the decaying turbulence after a merger. Alternatively, one could attempt to reconstruct the intrinsic high-frequency RH spectrum by filling in the missing flux due to the Sunyaev-Zel'dovich effect by precise measurements of the Compton-y parameter at microwave frequencies. Another possibility would consist in stacking the radio data of radio-quiet clusters that due not exhibit RH emission (Brown et al. 2011). This may reveal the glow of radio emission due to steady state secondary population. Emission from faint secondary electrons should still be visible, whereas due to the much more intermittent nature of DSA injection, primary CRe will instead show a sharp cutoff due to cooling, and will not be visible at high energies (see Fig. 5). We will pursue further implications and distinguishing characteristics of these competing models in future work.

Acknowledgments. We thank Josh Wiener for discussions on CR streaming. We are also grateful to Lawrence Rudnick for discussion on uncertainties in the 1.4 GHz radio data. Finally, we thank Fabio Zandanel for recalculating gamma-ray limits and Gianfranco Brunetti for useful discussions. A.P. is grateful to the Swedish research council for financial support. S.P.O. thanks NASA grant NNX12AG73G for support. C.P. gratefully acknowledges financial support of the Klaus Tschira Foundation.

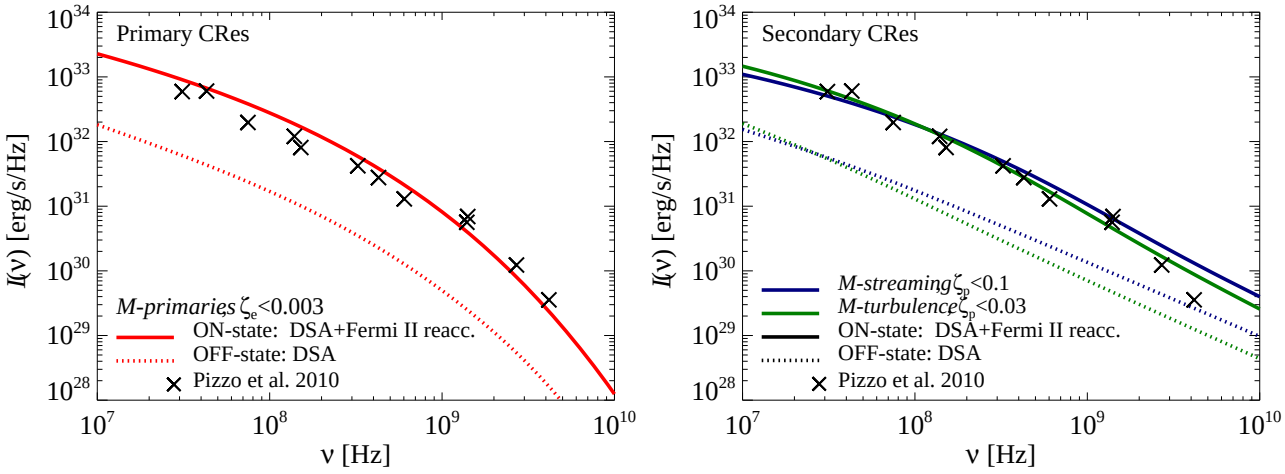

Figure 5. Radio synchrotron spectra. Lines are derived from simulations, while the black crosses are compiled from observations Pizzo (2010). The solid lines show the DSA and reaccelerated CRs (On-state of the radio halo), while the dotted lines show CRs accelerated only by DSA (Off-state of the radio halo). The left figure shows the radio emission induced by primary CRes and the right figure shows the emission from secondary CRes. The different line colors represent our different models, *M-primaries* (red line), *M-streaming* (blue line), and *M-turbulence* (green line).

REFERENCES

Ackermann M., et al., 2014, ApJ, 787, 18
Arlen T., et al., 2012, ApJ, 757, 123
Arnaud M., et al., 2001, A&A, 365, L67
Basu K., 2012, MNRAS, 421, L112
Battaglia N., Bond J. R., Pfrommer C., Sievers J. L., 2012, ApJ, 758, 74
Beresnyak A., Xu H., Li H., Schlickeiser R., 2013, ApJ, 771, 131
Blasi P., Colafrancesco S., 1999, Astroparticle Physics, 12, 169
Bonafede A., Feretti L., Murgia M., Govoni F., Giovannini G., Dallacasa D., Dolag K., Taylor G. B., 2010, A&A, 513, A30
Bonamente M., Lieu R., Bulbul E., 2009, ApJ, 696, 1886
Briel U. G., Henry J. P., Boehringer H., 1992, A&A, 259, L31
Brown S., Rudnick L., 2011, MNRAS, 412, 2
Brown S., Emerick A., Rudnick L., Brunetti G., 2011, ApJ, 740, L28
Brunetti G., Jones T. W., 2014, International Journal of Modern Physics D, 23, 30007
Brunetti G., Lazarian A., 2007, MNRAS, 378, 245
Brunetti G., Lazarian A., 2011, MNRAS, 412, 817
Brunetti G., Setti G., Feretti L., Giovannini G., 2001, MNRAS, 320, 365
Brunetti G., Blasi P., Cassano R., Gabici S., 2004, MNRAS, 350, 1174
Brunetti G., et al., 2008, Nature, 455, 944
Brunetti G., Blasi P., Reimer O., Rudnick L., Bonafede A., Brown S., 2012, MNRAS, 426, 956
Caprioli D., Spitkovsky A., 2014, ApJ, 783, 91
Chernyshov D. O., Dogiel V. A., Ko C. M., 2012, ApJ, 759, 113
Deiss B. M., Reich W., Lesch H., Wielebinski R., 1997, A&A, 321, 55
Dennison B., 1980, ApJ, 239, L93
Dolag K., Borgani S., Murante G., Springel V., 2009, MNRAS, 399, 497
Donnert J., Brunetti G., 2014, MNRAS, 443, 3564
Donnert J., Dolag K., Brunetti G., Cassano R., 2013, MNRAS, 429, 3564
Ellison D. C., Berezhko E. G., Baring M. G., 2000, ApJ, 540, 292
Enßlin T. A., 2002, A&A, 396, L17
Enßlin T., Pfrommer C., Miniati F., Subramanian K., 2011, A&A, 527, A99+
Farmer A. J., Goldreich P., 2004, ApJ, 604, 671
Feretti L., Giovannini G., Govoni F., Murgia M., 2012, A&ARv, 20, 54
Giovannini G., Feretti L., Venturi T., Kim K. T., Kronberg P. P., 1993, ApJ, 406, 399
Govoni F., Enßlin T. A., Feretti L., Giovannini G., 2001, A&A, 369, 441
Guo X., Sironi L., Narayan R., 2014a, ApJ, 794, 153
Guo X., Sironi L., Narayan R., 2014b, ApJ, 797, 47
Kang H., Ryu D., 2011, ApJ, 734, 18
Lau E. T., Kravtsov A. V., Nagai D., 2009, ApJ, 705, 1129
Miniati F., 2015, ApJ, 800, 60
Miniati F., Ryu D., Kang H., Jones T. W., 2001a, ApJ, 559, 59
Miniati F., Jones T. W., Kang H., Ryu D., 2001b, ApJ, 562, 233
Petrosian V., East W. E., 2008, ApJ, 682, 175
Pfrommer C., 2008, MNRAS, 385, 1242
Pfrommer C., Dursi L., 2010, Nature Physics, 6, 520
Pfrommer C., Enßlin T. A., 2004a, A&A, 413, 17
Pfrommer C., Enßlin T. A., 2004b, Astron. Astrophys., 426, 777
Pfrommer C., Enßlin T. A., Springel V., Jubelgas M., Dolag K., 2007, MNRAS, 378, 385
Pfrommer C., Enßlin T. A., Springel V., 2008, MNRAS, 385, 1211
Pinzke A., Pfrommer C., 2010, MNRAS, 409, 449
Pinzke A., Oh S. P., Pfrommer C., 2013, MNRAS, 435, 1061
Pizzo R. F., 2010, PhD thesis, University of Groningen
Planck Collaboration et al., 2013, A&A, 554, A140
Ruszkowski M., Lee D., Brüggen M., Parrish I., Oh S. P., 2011, ApJ, 740, 81
Sarazin C. L., 1999, ApJ, 520, 529
Schlickeiser R., Sievers A., Thiemann H., 1987, A&A, 182, 21
Shaw L. D., Nagai D., Bhattacharya S., Lau E. T., 2010, ApJ, 725, 1452
Vazza F., Brüggen M., 2014, MNRAS, 437, 2291
Vazza F., Brunetti G., Gheller C., Brunino R., Brüggen M., 2011, A&A, 529, A17
Vazza F., Gheller C., Brüggen M., 2014, MNRAS, 439, 2662
Wiener J., Oh S. P., Guo F., 2013, MNRAS, 434, 2209
Yan H., Lazarian A., 2002, Physical Review Letters, 89, 1102
Yan H., Lazarian A., 2004, ApJ, 614, 757
Zandanel F., Ando S., 2014, MNRAS, 440, 663
Zandanel F., Pfrommer C., Prada F., 2014, MNRAS, 438, 124
van Weeren R. J., Röttgering H. J. A., Brüggen M., Hoeft M.,

2010, Science, 330, 347